IOP Publishing Journal of Physics B: Atomic, Molecular and Optical Physics
J. Phys. B: At. Mol. Opt. Phys. **53** (2020) 095401 (8pp) https://doi.org/10.1088/1361-6455/ab76e5

Exceptional points enhancing second-order sideband generation in a whispering-gallery-mode microresonator optomechanical system coupled with nanoparticles

Xiao-Hu Lu, Liu-Gang Si[1], Xiao-Yun Wang and Ying Wu[1]

School of Physics, Huazhong University of Science and Technology, Wuhan, 430074, People's Republic of China

E-mail: siliugang@hust.edu.cn and yingwu2@126.com

Received 19 November 2019, revised 14 January 2020
Accepted for publication 17 February 2020
Published 31 March 2020

Abstract

We theoretically investigate the second-order sideband generation (SSG) in a whispering-gallery-mode (WGM) microresonator optomechanical system, in which the WGM microresonator couples with two nanoparticles. The nanoparticles can induce the optical coupling of the clockwise (CW) and the counterclockwise (CCW) WGM fields. And by continuously adjusting the relative phase angle between two nanoparticles, two eigenmodes of the optomechanical system coalesce and the so-called exceptional points (EPs) emerge periodically. It is shown that in the WGM microresonator optomechanical system coupled with nanoparticles in the second-order sideband can be generated due to the nonlinear optomechanical interactions, modulated periodically by the relative phase angle between two nanoparticles, and enhanced significantly at the EPs. Particularly, considering the frequency shift caused by the nanoparticles at the EPs, the generation and absorption of the second-order sideband can be flexibly realized. These results may have potential applications for high precision measurements and the manipulation of light propagation in optical cavities.

Keywords: cavity optomechanics, exceptional points, second-order sideband

(Some figures may appear in colour only in the online journal)

1. Introduction

Cavity optomechanics [1, 2] has attracted enormous interest to explore the interaction between light and matter, which takes advantage of the coupling between optical mode and mechanical mode via radiation pressure. Some remarkable results have been achieved, such as mechanical oscillator cooling [3], optomechanically induced transparency (OMIT)[4, 5], photon blockade [6, 7], non-classical state preparation [8–10], and non-destructive measurement [11]. In particular, as an important phenomenon in the exploration of optomechanically induced nonlinearity [12], OMIT has made significant progress in numerous systems, such as OMIT and slow light in parity-time-symmetric microresonators [13], double OMIT windows generated by coulomb interaction [14], OMIT in a membrane-in-the-middle system [15, 16], OMIT and absorption in hybridized optomechanical systems [17, 18].

Generally, OMIT is a linear and first-order sideband effect induced by the destructive interference between the optical fields in optomechanical systems. Second- and higher-order sidebands [19, 20] in OMIT is an interesting nonlinear optomechanical effect and has made some progress, such as quadrature squeezing of a higher-order sideband spectrum in cavity optomechanics [21] and the precision measurement of magnetic field based on the second-order sideband [22]. However, the higher-order sideband effect is weak under the weak coupling mechanism in optomechanical systems, which is generally ignored. Then some methods have been proposed to enhance higher-order sideband effects, such as amplifying

[1] Authors to whom any correspondence should be addressed.

higher-order sidebands in nonlinear optomechanics with gain and loss [23], enhanced generation of higher-order sidebands in a single-quantum-dot-cavity system coupled to a parity-time-symmetric double cavity [24], enhanced optomechanical second-order sidebands in a Kerr resonator [25] and enhanced second-order sideband generation in an optomechanical system with atom-cavity-resonator coupling [26].

Recently, the whispering-gallery-mode (WGM) microresonator [27] has aroused widespread concern due to its high quality factor and small volume mode. Because it is capable of storing light in the microscopic space for a long time, a strong enhancement of nonlinear interaction can be realized [28]. It has achieved fruitful results in fundamental physics and engineering applications, such as quantum-coherent coupling [29], low threshold lasers [30], biosensing [31, 32], optical frequency combs [33], sideband cooling [34], optomechanically induced non-reciprocal [35, 36]. Subsequently, the introduction of nanoparticles significantly improves the efficient of optomechanically induced nonlinearity [37–39]. And the effects of eigenfrequency shift and mode splitting [40, 41] caused by the interaction of nanoparticles and optical fields have important applications in optics and photonics, such as detection of nanoparticles [42, 43] and the design of the sensor [44]. In particular, when the nanoparticle-induced supermodel is degenerate, the so-called exceptional points (EPs) emerge and can significantly improve the sensitivity of detection [45]. At the EPs, some interesting phenomena have been revealed, such as chiral modes and directional lasing [46], phonon laser [47, 48] and OMIT [49].

Motivated by recent theoretical and experimental research results [46, 47], we study the second-order sideband generation (SSG) in a WGM microresonator optomechanical system, in which two nanoparticles are coupled to the WGM microresonator. The existance of nanoparticles induces the optical coupling of the clockwise- (CW) and the counterclockwise-(CCW) WGM fields. Then the EPs emerge periodically by continuously adjusting the relative phase angle between two nanoparticles where two eigenmodes of the optomechanical system coalesce. Our results show that in the WGM microresonator optomechanical system coupled with nanoparticles the second-order sideband can be generated due to the nonlinear optomechanical interactions, modulated periodically by the relative phase angle between two nanoparticles, and enhanced significantly at the EPs. Meanwhile, at the EPs, the optomechanical system can realize the transformation of OMIT and second-order sideband by adjusting the detuning of the cavity field and the control field. Extraordinary, the optomechanical system has more stable transmission characteristics under the EPs mechanism. This is beneficial for us to prepare optical transmission quantum devices.

The paper is organized as follows. In section 2, the general model of the the WGM microresonator optomechanical system and the Hamiltonian are given. We introduce the processing method to deal with the Hamiltonian and obtain the expressions to describe the OMIT and SSG. In section 3, the characteristics of OMIT and SSG in the optomechanical system at the EPs are analyzed and the influence of the system parameters on the OMIT and SSG is discussed in detail. We made a brief summary in section 4.

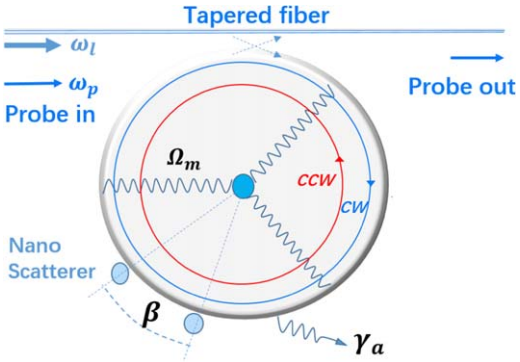

Figure 1. Sketch of the optomechanical system. A WGM microresonator (damping rate γ_a) couples with two nanoparticles, which is driven by a strong control field with frequency ω_l and a weak probe field with frequency ω_p. CW and CCW are the clockwise and counterclockwise rotating intracavity fields. Ω_m is the mechanical frequency of the phonon mode. β is the relative phase angle between two nanoparticles.

2. Theoretical model and formulations

The optomechanical system we consider is a silica microtoroid WGM microresonator coupled with two nanoparticles. The nanoparticles are two silica nanotips that are placed near the boundary of the WGM resonator. When a strong control field (with the amplitudes $\varepsilon_l = \sqrt{P_l/\hbar\omega_l}$) and a weak probe field (with the amplitudes $\varepsilon_p = \sqrt{P_p/\hbar\omega_p}$) are injected into the cavity, the optomechanical system is excited by a tapered fiber coupled to the WGM microresonator, as shown in figure 1. P_l and P_p denote the powers of the control field and the probe field, respectively. Due to the presence of nanoparticles, the optical mode can backscatter into clockwise (CW) and counterclockwise(CCW) propagating modes and form instantaneous coupling [50, 51]. The coupling strength can be approximately treated as $J_{1,2} = \epsilon_1 + \epsilon_2 e^{\mp i2m\beta}$, where ϵ_1 and ϵ_2 are given by the complex frequency shifts for positive-parity and negative-parity modes introduced by i-th particle ($i = 1, 2$) alone. They can be changed by adjusting the position and size of the nanoparticles. m is the azimuthal mode number, and β is the relative phase angle between two nanoparticles.

Now, we can write the Hamiltonian formulation of the whole system in the rotating frame at the frequency ω_l of the control field [49],

$$\begin{aligned} H = {} & \hbar\Delta(a_{CW}^{\dagger}a_{CW} + a_{CCW}^{\dagger}a_{CCW}) \\ & + \frac{p^2}{2m} + \frac{1}{2}m_{eff}\Omega_m^2 x^2 \\ & + \hbar J_1 a_{CW}^{\dagger}a_{CCW} + \hbar J_2 a_{CCW}^{\dagger}a_{CW} \\ & - \hbar g x(a_{CW}^{\dagger}a_{CW} + a_{CCW}^{\dagger}a_{CCW}) \\ & + i\hbar\sqrt{\gamma_{ex}}((\varepsilon_l + \varepsilon_p e^{-i\Omega t})a_{CW}^{\dagger} - H.c.), \end{aligned} \tag{1}$$

where the first term is the free Hamiltonian of the cavity field, the second and third terms are the free Hamiltonian of the mechanical mode, the fourth and fifth terms are the interactions between optical modes a_{CW} and a_{CCW}, and the sixth term is the interaction of mechanical mode and optical mode,

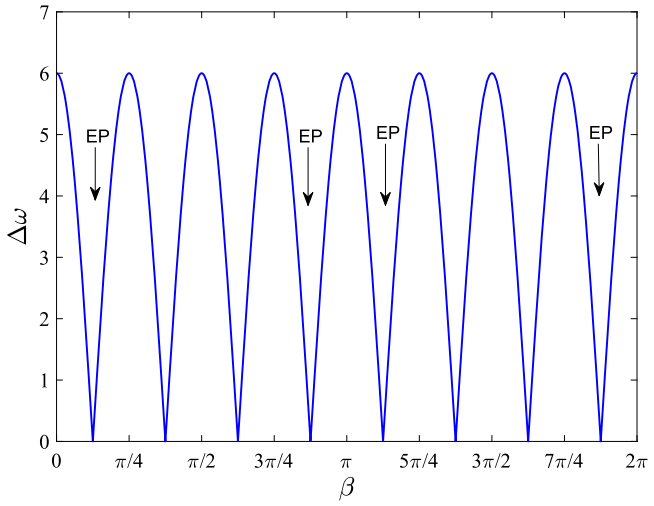

Figure 2. The splitting frequency $\Delta\omega$ as a function of the relative phase angle β.

and the last term is the driving term. And, a_{CW} (a_{CCW}) and $a_{CW}^{\dagger}$ ($a_{CCW}^{\dagger}$) represent the bosonic annihilation and creation operators of the CW (CCW) mode, p and x are the momentum operator and position operator of the mechanical mode (with the effective mass m_{eff} and the angular frequency Ω_m), γ_{ex} is the loss rate from the tapered fiber coupled to the WGM microresonator. The coupling constant between the optical mode and the mechanical mode is defined as $g = \omega_a/R$, where ω_a and R is the resonance frequency and radius of the WGM resonator, respectively. And, $\Delta = \Delta_a + \mathrm{Re}(\epsilon_1 + \epsilon_2)$, where $\Delta_a = \omega_a - \omega_l$ is the detuning frequency between the cavity field and the control field, and the term $\mathrm{Re}(\epsilon_1 + \epsilon_2)$ is derived from the modulation of nanoparticles. The detuning frequency between the probe field and the control field is $\Omega = \omega_p - \omega_l$.

When the nanoparticles are placed in the optical cavity, Rayleigh scattering is formed on the surface of the nanoparticles, which leads to the coupling between the CW mode and the CCW mode. For simplicity, we can get the effective Hamiltonian of the optical cavity field as

$$\begin{aligned} H_{eff} = &(\omega_a - i\gamma)a_{CW}^{\dagger}a_{CW} + (\omega_a - i\gamma)a_{CCW}^{\dagger}a_{CCW} \\ &+ \hbar J_1 a_{CW}^{\dagger}a_{CCW} + \hbar J_2 a_{CCW}^{\dagger}a_{CW} \end{aligned} \tag{2}$$

and the corresponding eigenfrequency can be obtained as

$$\begin{aligned} \omega_{\pm} = &\omega_a - i\gamma_a + \epsilon_1 + \epsilon_2 \\ &\pm\sqrt{\epsilon_1^2 + \epsilon_2^2 + 2\epsilon_1\epsilon_2 cos(2m\beta)}\,. \end{aligned} \tag{3}$$

From equation (3), the two optical modes induced by the nanoparticles can split into two supermodes, the two supermodes's splitting frequency $\Delta\omega$ can be periodically modulated by tuning the angle β(as shown in figure 2). Particularly, the supermodes's splitting frequency $\Delta\omega$ is zero at $\beta = n\pi/8$ ($n = 1, 3, 5, \ldots$) . This is mainly because the nanoparticles induce the appearance of EPs [49, 52]. In figure 2, there are two EPs in the interval of 0 to $\pi/2$, which are $\beta = \pi/8$ ($\beta \approx 0.4$), $\beta = 3\pi/8$($\beta \approx 1.2$). At EPs, the eigenfrequency of the two supermodes is degenerate. The system's EPs are obtained by continuously adjusting β to get $J_2 = 0$. At this condition, the scattering from the CW to CCW modes is prohibited. The EPs effect has achieved extensive research results in the cavity optomechanical system, such as topological energy transfer effect [53], the low-power phonon laser [47], enhanced sensitivity at exceptional points [45] and higher-order exceptional points [54].

In the present work, we are interested in the mean response of the system to the probe field by ignoring quantum and thermal noise terms [1]. Considering the loss of the cavity field and the resonator, the simplified Heisenberg-Langevin equations can be written as

$$\begin{aligned} \dot{a}_{CW} = &(-i\Delta + igx - \gamma)a_{CW} - iJ_1 a_{CCW} \\ &+ \sqrt{\gamma_{ex}}\varepsilon_l + \sqrt{\gamma_{ex}}\varepsilon_p e^{-i\Omega t}, \\ \dot{a}_{CCW} = &(-i\Delta + igx - \gamma)a_{CCW} - iJ_2 a_{CW}, \\ \dot{x} = &\, p/m_{eff}, \\ \dot{p} = &-m_{eff}\Omega_m^2 x \\ &- \hbar g(a_{CW}^{\dagger}a_{CW} + a_{CCW}^{\dagger}a_{CCW}) - \gamma_m p, \end{aligned} \tag{4}$$

where $\gamma = \gamma_a - \mathrm{Im}(\epsilon_1 + \epsilon_2)$ is the total optical loss, γ_m is the decay rate of the WGM resonator. Considering that the power of the control field is much larger than the probe field, we use the perturbation method to deal with the dynamic equations. Then, equation (4) can be solved by using $A = \overline{A} + \delta A$, where $\overline{A}$ is the steady-state term and δA is the perturbation term. Thus, the steady-state terms can be solved as

$$\begin{aligned} \overline{x} &= \frac{\hbar g}{m_{eff}\Omega_m^2}(|\overline{a_{CW}}|^2 + |\overline{a_{CCW}}|^2), \\ \overline{a_{CW}} &= \frac{-\sqrt{\gamma_{ex}}\varepsilon_l(-i\Delta + ig\overline{x} - \gamma)}{(-i\Delta + ig\overline{x} - \gamma)^2 + J_1 J_2}, \\ \overline{a_{CCW}} &= \frac{-iJ_2\sqrt{\gamma_{ex}}\varepsilon_l}{(-i\Delta + ig\overline{x} - \gamma)^2 + J_1 J_2}, \end{aligned} \tag{5}$$

and the fluctuation terms can be written as

$$\begin{aligned} \frac{d}{dt}\delta a_{CW} = &(-i\Delta + ig\overline{x} - \gamma)\delta a_{CW} - iJ_1\delta a_{CWW} \\ &+ ig(\overline{a_{CW}}\delta x + \delta x\delta a_{CW}) + \sqrt{\gamma_{ex}}\varepsilon_p e^{-i\Omega t}, \\ \frac{d}{dt}\delta a_{CCW} = &(-i\Delta + ig\overline{x} - \gamma)\delta a_{CCW} - iJ_2\delta a_{CW} \\ &+ ig(\overline{a_{CCW}}\delta x + \delta x\delta a_{CCW}), \\ \widehat{\Psi}\delta x = &\frac{\hbar g}{m_{eff}}(\overline{a_{CW}}^{*}\delta a_{CW} + \overline{a_{CW}}\delta a_{CW}^{*} \\ &+ \delta a_{CW}^{*}\delta a_{CW} \\ &+ \overline{a_{CCW}}^{*}\delta a_{CCW} + \overline{a_{CCW}}\delta a_{CCW}^{*} \\ &+ \delta a_{CCW}^{*}\delta a_{CCW}), \end{aligned} \tag{6}$$

where $\widehat{\Psi} = \frac{d^2}{dt^2} + \gamma_m\frac{d}{dt} + \Omega_m^2$. In previous studies, many people often overlooked the impact of higher-order nonlinear terms on the system. In equation (6), we retain the higher-order nonlinear terms $\delta x\delta a_{CW}$, $\delta x\delta a_{CCW}$, $\delta a_{CW}^{*}\delta a_{CW}$ and $\delta a_{CCW}^{*}\delta a_{CCW}$, which result in the generation of the second- and higher-order sideband.

We analyze the output spectral properties of the probe field by using the following ansatz:

$$\begin{aligned}\delta a_{CW} &= A_1^- e^{-i\Omega t} + A_1^+ e^{i\Omega t} + A_2^- e^{-2i\Omega t} + A_2^+ e^{2i\Omega t}\\ \delta a_{CWW} &= B_1^- e^{-i\Omega t} + B_1^+ e^{i\Omega t} + B_2^- e^{-2i\Omega t} + B_2^+ e^{2i\Omega t}\\ \delta x &= X_1 e^{-i\Omega t} + X_1^* e^{i\Omega t} + X_2 e^{-2i\Omega t} + X_2^* e^{2i\Omega t}\end{aligned} \tag{7}$$

where A_n^- and A_n^+ are the amplitudes of the nth-order higher upper and lower sidebands, respectively. Extraordinarily, there are the output fields with frequencies $\omega_l \pm n\Omega$ (n is a integer) generated, which results from the nonlinear terms $ig(\delta x \delta a_{CW} + \delta x \delta a_{CCW})$ and $\frac{\hbar g}{m_{eff}}(\delta a_{CW}^* \delta a_{CW} + \delta a_{CCW}^* \delta a_{CCW})$. Here, we focus on the second-order sideband effect in the system, ignoring other higher-order sidebands. Substituting equation (7) into equation (6), we can obtain some parameters we are interested in:

$$\begin{aligned}A_1^- &= \frac{\sqrt{\gamma_{ex}}\varepsilon_p U_1(R(\Omega)S_2U_1U_2 - \hbar g^2 G_2)}{\alpha - \hbar g^2(S_1G_2 + U_2S_2G_1)},\\ X_1 &= \frac{\sqrt{\gamma_{ex}}\varepsilon_p \hbar g U_1U_2S_2G_1}{(i\bar{a}_1U_1 + \bar{a}_2J_1)(\alpha - \hbar g^2(S_1G_2 + U_2S_2G_1))},\\ A_2^- &= \frac{\hbar g^2(i\bar{a}_1U_3 + J_1\bar{a}_2)(E_1 + E_2) + E_3}{R(2\Omega)S_3S_4U_3U_4 - \hbar g^2(S_3G_4 + U_4S_4G_3)},\end{aligned} \tag{8}$$

where

$$\begin{aligned}\alpha &= R_1S_1S_2U_1U_2, \quad U_{1,2} = -i\Omega \pm (i\Delta - ig\bar{x}) + \gamma\\ U_{3,4} &= -2i\Omega \pm (i\Delta - ig\bar{x}) + \gamma\\ S_{1,3} &= U_{1,3}^2 + J_1J_2, \quad S_{2,4} = U_{2,4}^2 + J_1^*J_2^*\\ R(\Omega) &= m_{eff}(-\Omega^2 - i\Omega\gamma_m + {\Omega_m}^2)\\ G_{1,3} &= i(U_{1,3}^2|\bar{a}_1|^2 - J_1J_2|\bar{a}_2|^2)\\ &\quad + U_{1,3}(J_1\bar{a}_1^*\bar{a}_2 + J_2\bar{a}_1\bar{a}_2^*)\\ G_{2,4} &= 2S_{2,4}V_1 - iU_{1,3}V_{2,4}\\ &\quad + U_{1,3}U_{2,4}(J_1^*\bar{a}_1\bar{a}_2^* + J_2^*\bar{a}_2\bar{a}_1^*)\\ V_1 &= (\Delta - g\bar{x})|\bar{a}_2|^2,\\ V_{2,4} &= U_{2,4}^2|\bar{a}_1|^2 - J_1^*J_2^*|\bar{a}_2|^2\end{aligned} \tag{9}$$

and $E_1 = U_3U_4S_4((A_1^+)^*A_1^- + (B_1^+)^*B_1^-)$, $E_2 = gX_1(i\bar{a}_2^*U_4S_4B_1^- + U_3(J_1^*\bar{a}_1U_4 + i\bar{a}_2(J_1^*J_2^* - S_4))(B_1^+)^* - U_3U_4(iU_4\bar{a}_1 - J_2^*)(A_1^+)^*)$, $E_3 = gX_1(R_2S_4U_3U_4 - \hbar g^2G_4)(J_1B_1^- + iU_3A_1^-)$, $B_1^- = \frac{ig\bar{a}_2X_1 - J_2A_1^-}{U_1}$, $(B_1^+)^* = \frac{-gX_1(-i\bar{a}_2^*S_2 - J_2^*(\bar{a}^*{}_1U_2 + iJ_1^*\bar{a}_2^*))}{U_2S_2}$, $(A_1^+)^* = \frac{-gX_1(i\bar{a}_2^*U_2 - J_1^*\bar{a}_2^*)}{S_2}$.

By using the input-output relationship $S_{out} = S_{in}(t) - \sqrt{\gamma_{ex}}a$, we obtain the output field

$$\begin{aligned}S_{out} &= (\varepsilon_l - \sqrt{\gamma_{ex}}\bar{a})e^{-i\omega_l t}\\ &\quad + (\varepsilon_p - \sqrt{\gamma_{ex}}A_1^+)e^{-i(\omega_l+\Omega)t}\\ &\quad - \sqrt{\gamma_{ex}}A_1^- e^{-i(\omega_l-\Omega)t}\\ &\quad - \sqrt{\gamma_{ex}}A_2^+ e^{-i(\omega_l+2\Omega)t} - \sqrt{\gamma_{ex}}A_2^- e^{-i(\omega_l-2\Omega)t}\\ &= c_l e^{-i\omega_l t} + c_p e^{-i\omega_p t} - \sqrt{\gamma_{ex}}A_2^- e^{-i(2\omega_p-\omega_l)t}\\ &\quad - \sqrt{\gamma_{ex}}A_1^+ e^{-i(2\omega_l-\omega_p)t} - \sqrt{\gamma_{ex}}A_2^+ e^{-i(3\omega_l-2\omega_p)t},\end{aligned} \tag{10}$$

where $c_l = \varepsilon_l - \sqrt{\gamma_{ex}}\bar{a}$, $c_p = \varepsilon_p - \sqrt{\gamma_{ex}}A_1^-$, $\omega_p = \omega_l + \Omega$. The terms $c_l e^{-i\omega_l t}$ and $c_p e^{-i\omega_p t}$ are the response of the output fields at the frequency ω_l and ω_p, respectively. The term $-\sqrt{\gamma_{ex}}A_1^+ e^{-i(2\omega_l-\omega_p)t}$ describes the Stokes field process. The terms $-\sqrt{\gamma_{ex}}A_2^- e^{-i(2\omega_p-\omega_l)t}$ and $-\sqrt{\gamma_{ex}}A_2^+ e^{-i(3\omega_l-2\omega_p)t}$ describe the second-order upper sideband process and the second-order lower sideband process, in which the output field with frequency $\omega_l \pm 2\Omega$ can be produced. The transmission rate of the probe field and the efficiency of generating the second-order sideband are defined as

$$\begin{aligned}|t_p|^2 &= |\frac{c_p}{\varepsilon_p}|^2 = |1 - \sqrt{\eta_c\gamma}A_1^-/\varepsilon_p|^2\\ \eta &= |-\sqrt{\eta_c\gamma}A_2^-/\varepsilon_p|^2.\end{aligned} \tag{11}$$

Next, the efficiency of SSG in the optomechanical system will be discussed. The main parameters we use are from recent experiments [46, 55], as follows: $R = 34.5\mu$m, $m_{eff} = 50$ ng, $\omega_m = 2\pi \times 23.4$ MHz, $\omega_a = 2\pi \times 193$ THz, $\gamma_a = 6.45$ MHz, $\gamma_{ex} = 12.9$ MHz, $\gamma_m = 0.24$ MHz, $\epsilon_1 = \gamma_a \times (1.5 - 0.1i)$, $\epsilon_2 = \gamma_a \times (1.4999 - 0.101489i)$, $m = 4$.

3. Results and discussion

In this section, we will numerically calculate the transmission rate of the probe field and the efficiency of the second-order sideband as functions of some system parameters. We focus on the impact of EPs on the system, and discuss the efficiency of SSG by continuously adjusting the relative phase angle between two nanoparticles to reach the EPs. The results will show that the second-order sideband can be generated and enhanced at EPs.

Firstly, based on the importance of the position of two nanoparticles, we will discuss the influence of the relative phase angle β between two nanoparticles on the optomechanical system. It is shown in figure 3(a) that the transmission rate ($|t_p^2|$) is the periodic function of the relative phase angle β. And, we can clearly observe that with the change of β, the optical mode of the system is degenerated from the two modes into a mode. At $\beta = 0.4$ and $\beta = 1.2$, the supermodes's splitting frequency $\Delta\omega$ is zero, and the nanoparticles induce the appearance of EPs. Particularly, the transmission rate ($|t_p^2|$) can be significantly enhanced at $\beta = 0.4$ and $\beta = 1.2$. It is mainly because the eigenfrequency of the two supermodes is degenerate at EPs, this effectively improves the coupling of optical and mechanical modes and enhances the efficiency of the second-order sideband. As shown in figure 3(b), the second-order sideband occurs near the resonance condition $\Delta = \Omega_m$. The relative phase angle β has also a periodic modulation effect on the second-order sideband. Just at the EPs, i.e. $\beta = 0.4$ and $\beta = 1.2$, the efficiency of SSG reaches the maximum. When there is only one nanoparticle, i.e. $\beta = 0$ and $\beta = 0.8$, the efficiency of SSG is very weak. And, the efficiency of SSG is shown in figure 3(c) as a function of the relative phase angle β from 0 to 0.4. It can be found that the second-order sideband is very weak when it is

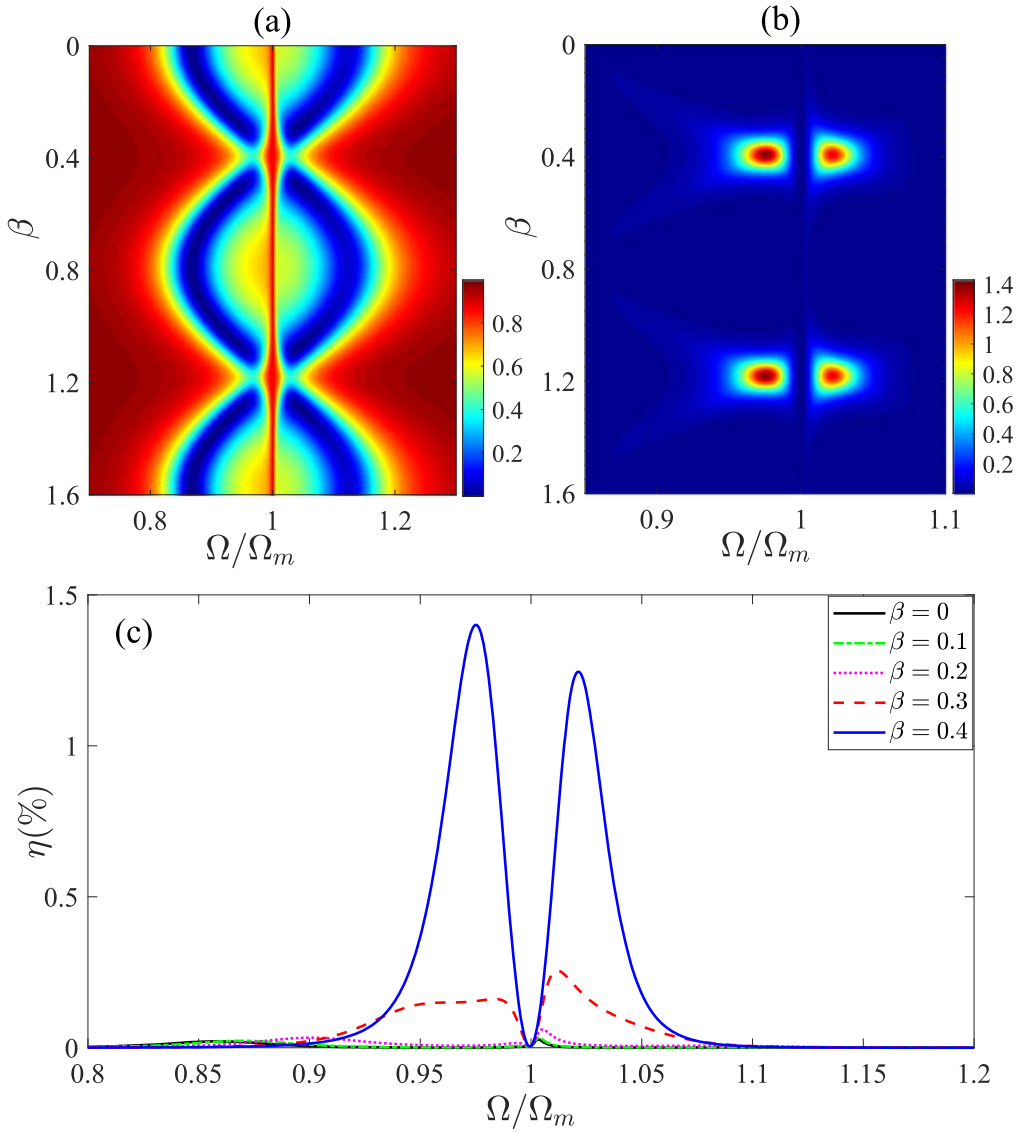

Figure 3. (a) Plot of the transmission rate ($|t_p^2|$) of the probe field as a function of the relative phase angle β and the detuning frequency Ω. (b) Plot of the efficiency η of SSG as a function of β and Ω. (c) Plot of the efficiency η of SSG vs Ω for different values of β. Other parameters are given by $\Delta = \Omega_m$, $P_l = 0.55$mW.

far from the EPs. Extraordinarily, the second-order sideband is absorbed at $\Omega = \Omega_m$ and two peaks are formed when $\beta = 0.2$. Then, the second-order sideband reaches the maximum value at the EPs, i.e. $\beta = 0.4$. Therefore, the system can achieve periodic modulation to generate the second-order sideband which is significantly enhanced at the EPs.

Secondly, considering the EPs effect, we will show that the output of the probe field is very sensitive to the detuning frequency of the cavity field and the control field. The detuning frequency between the cavity field and the control field we consider is $\Delta_a = \omega_a - \omega_l$. As shown in figure 4(a), when the effects of EPs are considered, the OMIT window takes place at the resonance conditions $\Delta = \Omega_m$ and $\Omega = \Omega_m$. At this condition, the detuning frequency of the control field and the probe field is $\Delta_a = \Omega_m -$ Re$(\epsilon_1 + \epsilon_2)$, the term Re$(\epsilon_1 + \epsilon_2)$ is caused by the frequency shift induced by the nanoparticles. Theoretically, the generation of the second-order sideband is mainly from the upconverted first-order sideband. When the transmission rate $|t_p^2|$ of the probe field reaches the maximum, the second-order sideband is completely absorbed, as shown in figure 4(b). When we choose the detuning frequency $\Delta_a = \Omega_m$ between the cavity field and the control field, the transmission rate $|t_p^2|$ of the probe field is completely absorbed near the resonance condition $\Omega = \Omega_m$, as shown in figure 4(c). However, the efficiency of SSG reaches the maximum as shown in figure 4(d). It means that the optomechanical system can generate the second-order sideband at EPs when the resonance condition meet $\Delta_a = \Omega_m$. This mainly results from the EPs effect. At the EPs, the supermodes ω_+ degenerate with supermodel ω_-. And, the amplitude of the supermodes is small due to OMIT. Hence, the phonon amplitude becomes the largest among the three modes. It is conducive to enhance nonlinear effects. Reasonably using the frequency shift caused by nanoparticles

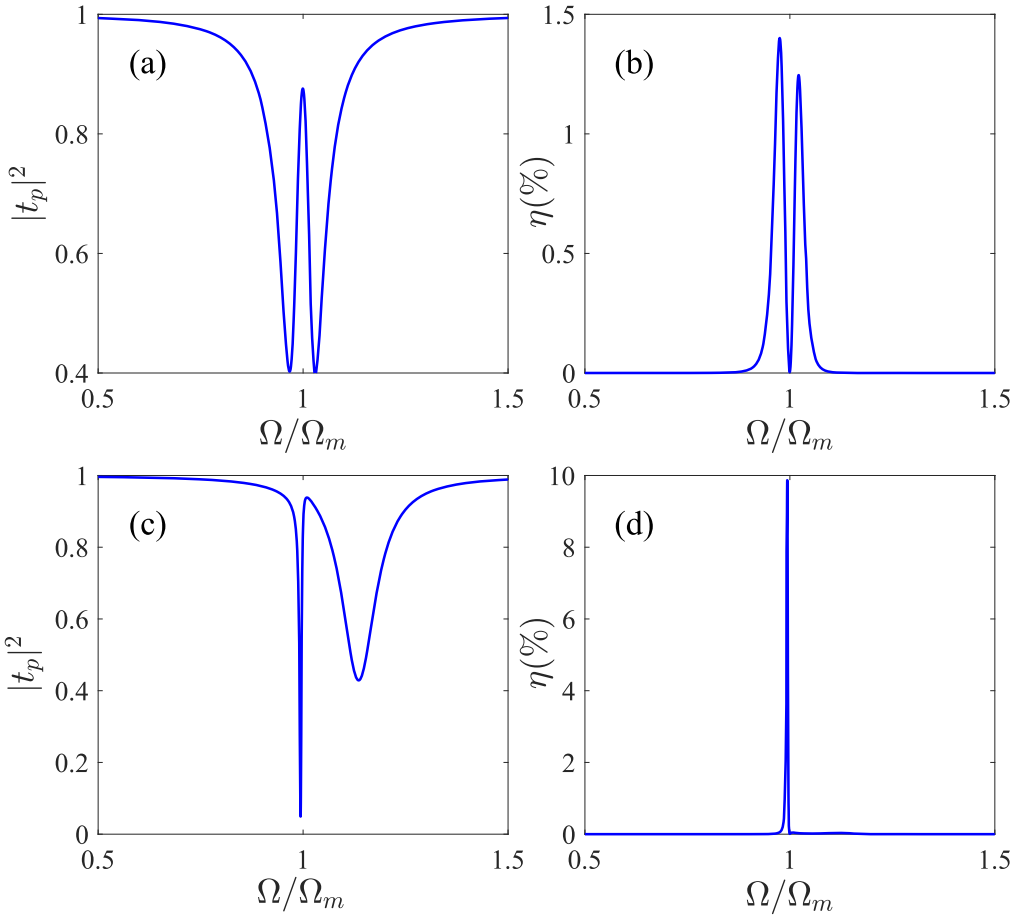

Figure 4. Plot the transmission rate ($|t_p^2|$) and the efficiency (η) of SSG as a function of the detuning frequency Ω. In panels (a) and (b), we use $\Delta = \Omega_m$, and in panels (c) and (d), we use $\Delta_a = \Omega_m$. The rest parameters are given by $\beta = 0.4$, $P_l = 0.55$mW.

at EPs, the system can achieve a second-order sideband and OMIT effective conversion.

Next, we discuss how to enhance the efficiency of SSG. As shown in figure 5(a), when the control field and the probe field satisfy the resonance condition $\Delta_a = \Omega_m$, the relative phase angle β can still periodically modulate the efficiency of SSG. Significantly, the difference between figures 3(b) and 5(a) is that the second-order sideband is absorbed and generated near $\Omega = \Omega_m$, respectively. This fits well with the properties of the optomechanical system at EPs. In figure 5(b), we plot the efficiency η of SSG varying from $\beta = 0$ to $\beta = 0.8$. When $\beta = 0$, the second-order sideband is absorbed near $\Omega = \Omega_m$, and there are two peaks. When $\beta = 0.2$, the second-order sideband has only one peak, and the peak on the right side of $\Omega = \Omega_m$ is absorbed. This shows that two nanoparticles induce the generation of the second-order sideband at EPs. Obviously, when $\beta = 0.4$, the amplitude of the second-order sideband has a significant enhancement. This is an interesting phenomenon that occurs at EPs. In addition, the intensity of the second-order sidebands can be enhanced by appropriately adjusting the power of the control field, as shown in figure 5(c). Similarly, in figure 5(d), the second-order sideband increases as the power of the control field increases at EPs. Thus, adjusting the power of the control field can enhance the amplitude of the second-order sideband. Comparing figures 5(c) with (d), we can find that the frequency offset of the second-order sideband at EPs is small, which is beneficial for highly precise measurements. Notice that the phenomenon that the spectrum of second-order sideband is shifted to the left at EPs as the power of the control field increasing is mainly due to the enhancement of the optomechanical coupling.

4. Conclusion

In conclusion, we have numerically studied a non-Hermitian optomechanical system to generate and enhance SSG at EPs. The effect of EPs induced by the introduction of nanoparticles on the optomechanical system are discussed. Theoretical analysis and numerical simulation results show that periodic modulation of SSG can be achieved by adjusting the relative phase β between two nanoparticles. In addition, considering the detuning frequency between the cavity and control fields

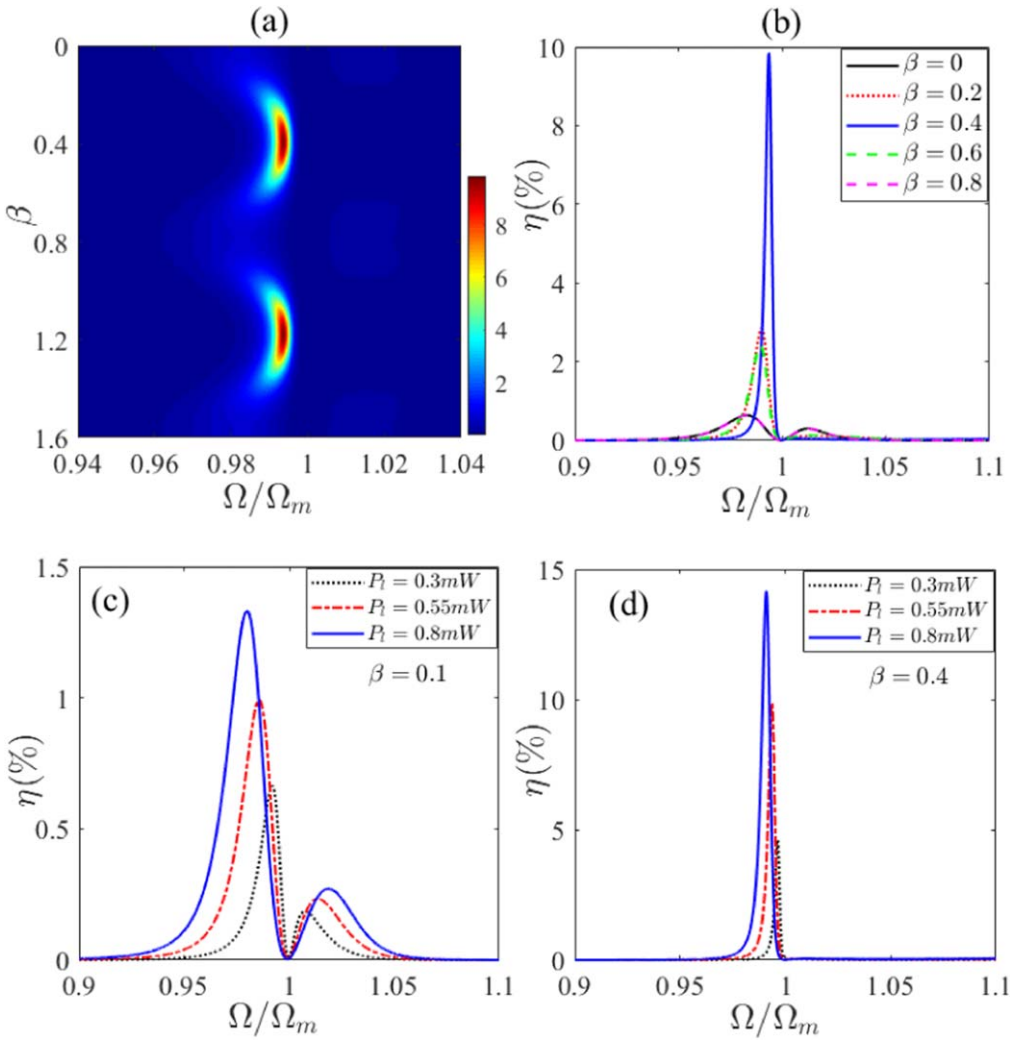

Figure 5. (a) Plot of the efficiency η of SSG as a function of the relative phase angle β and the detuning frequency Ω under $\Delta_a = \Omega_m$. (b) Plot of the efficiency η of SSG vs Ω for different values of β. The rest of the parameters are given by $\Delta_a = \Omega_m$, $P_l = 0.55$mW. And, the plot of the efficiency η of SSG vs Ω for different values of P_l with (c) $\beta = 0.1$, (d) $\beta = 0.4$. Other parameters are given by $\Delta = \Omega_m$.

at the EPs, flexible conversion between second-order sideband and OMIT can be achieved. These results may find potential applications in high precision measurements and manipulation of light propagation in optical cavities.

Acknowledgments

The work is supported in part by the National Key Research and Development Program of China (Grant No. 2016YFA0301203), the National Science Foundation of China (NSFC) (Grants Nos. 11975103, 11875029 and 11574104), and the Fundamental Research Funds for the Central Universities HUST (2018KFYYXJJ032).

ORCID iDs

Xiao-Hu Lu https://orcid.org/0000-0002-4427-0331

References

[1] Aspelmeyer M, Kippenberg T L and Marquardt F 2014 *Rev. Mod. Phys.* **86** 1391
[2] Metcalfe M 2014 *Appl. Phys. Rev.* **1** 031105
[3] Marquardt F, Chen J P, Clerk A A and Girvin S M 2007 *Phys. Rev. Lett.* **99** 093902
[4] Weis S, Rivière R, Deléglise S, Gavartin E, Arcizet O, Schliesser A and Kippenberg T J 2010 *Science* **330** 1520–3
[5] Dong C H, Shen Z, Zou C L and Guo G C 2015 *Sci. China. Phys. Mech. Astron.* **58** 050308
[6] Rabl P 2011 *Phys. Rev. Lett.* **107** 063601
[7] Liao J Q and Nori F 2013 *Phys. Rev.* A **88** 023853
[8] Teufel J D, Donner T, Li D L, Harlow J W, Allman M S, Cicak K, Sirois A J, Whittaker J D, Lehnert K W and Simmonds R W 2011 *Nature* **475** 359–63
[9] Dong C H, Fiore V, Kuzyk M C and Wang H L 2012 *Science* **338** 1609–13
[10] Palomaki T A, Teufel J D, Simmonds R W and Lehnert K W 2013 *Science* **342** 710–3
[11] Clerk A A, Marquardt F and Jacobs K 2008 *New. J. Phys.* **10** 095010

[12] Kronwald A and Marquardt F 2013 *Phys. Rev. Lett.* **111** 133601
[13] Jing H, Özdemir Ş K, Geng Z, Zhang J, Lü X Y, Peng B, Yang L and Nori F 2015 *Sci. Rep.* **5** 9663
[14] Ma P C, Zhang J Q, Xiao Y, Feng M and Zhang Z M 2014 *Phys. Rev.* A **90** 043825
[15] Huang S M and Agarwal G S 2011 *Phys. Rev.* A **83** 023823
[16] Karuza M, Biancofiore C, Bawaj M, Molinelli C, Galassi M, Natali R, Tombesi P, Giuseppe G D and Vitali D 2013 *Phys. Rev.* A **88** 013804
[17] Hou B P, Wei L F and Wang S J 2015 *Phys. Rev.* A **92** 033829
[18] Lu X H, Si L G, Wang B, Wang X Y and Wu Y 2019 *J. Phys. B: At. Mol. Opt. Phys.* **52** 085401
[19] Xiong H, Si L G, Zheng A S, Yang X X and Wu Y 2012 *Phys. Rev.* A **86** 013815
[20] Xiong X R, Gao Y P, Liu X F, Cao C, Wang T J and Wang C 2018 *Sci. China. Phys. Mech. Astron.* **61** 90322
[21] Liu S P, Yang W X, Zhu Z H, Shui T and Li L 2018 *Opt. Lett.* **43** 9–12
[22] Liu Z X 2018 *IEEE. Sens.* J **18** 22
[23] Jiao Y, Lü H, Qian J, Li Y and Jing H 2016 *New. J. Phys.* **18** 083034
[24] Yang W X, Chen A X, Xie X T and Ni L Y 2017 *Phys. Rev.* A **96** 013802
[25] Jiao Y F, Lu T X and Jing H 2018 *Phys. Rev.* A **97** 013843
[26] Chen B, Shang L, Wang X F, Chen J B, Xue H B, Liu X and Zhang J 2019 *Phys. Rev.* A **99** 063810
[27] PÖllinger M, O'Shea D, Warken F and Rauschenbeutel A 2009 *Phys. Rev. Lett.* **103** 053901
[28] Ilchenko V S, Savchenkov A A, Matsko A B and Maleki L 2004 *Phys. Rev. Lett.* **92** 043903
[29] Verhagen E, Deléglise S, Weis S, Schliesser A and Kippenberg T J 2012 *Nature* **482** 63–7
[30] Spillane S M, Kippenberg T J and Vahala K J 2002 *Nature* **415** 621–3
[31] Vollmer F and Arnold S 2008 *Nat. Methods* **5** 591–6
[32] Vollmer F, Arnold S and Keng D 2008 *Proc. Natl. Acad. Sci.* **105** 20701–4
[33] Savchenkov A A, Matsko A B, Ilchenko V S, Solomatine I, Seidel D and Maleki L 2008 *Phys. Rev. Lett.* **101** 093902
[34] Schliesser A, Arcizet O, Riviere R and Kippenberg T J 2009 *Nat. Phys.* **5** 509–14
[35] Hafezi M and Rabl P 2012 *Opt. Express* **20** 7672–84
[36] Shen Z, Zhang Y L, Chen Y, Zou C L, Xiao Y F, Zou X B, Sun F W, Guo G C and Dong C H 2016 *Nat. Photonics* **10** 657–61
[37] Zhu J G, Özdemir Ş K, Xiao Y F, Li L, He L N, Chen D R and Yang L 2010 *Nat. Photonics* **4** 46–9
[38] Shu F J, Jiang X F, Zhao G M and Yang L 2018 *Nat. Photonics* **7** 1455–60
[39] Yu X C, Liu Y C, Yan M Y, Jin W L and Xiao Y F 2012 *Phys. Rev.* A **86** 043833
[40] Zhu J G, Özdemir Ş K, He L N and Yang L 2010 *Opt. Express* **18** 23535–43
[41] Mazzei A, Götzinger S, Menezes L, de S, Zumofen G, Benson O and Sandoghdar V 2007 *Phys. Rev. Lett.* **99** 173603
[42] Swaim J D, Knittel J and Bowen W P 2013 *Appl. Phys. Lett.* **102** 183106
[43] Li B B, Clements W R, Yu X C, Shi K, Gong Q H and Xiao Y F 2014 *Proc. Natl. Acad. Sci.* **111** 14657–62
[44] Foreman M R, Swaim J D and Vollmer F 2015 *Adv. Opt. Photonics* **7** 168–240
[45] Chen W J, Özdemir Ş K, Zhao G M, Wiersig J and Yang L 2017 *Nature* **548** 192–6
[46] Peng B, Özdemir Ş K, Liertzer M, Chen W J, Kramer J, Yilmaz H, Wiersig J, Rotter S and Yang L 2016 *Proc. Natl. Acad. Sci.* **113** 6845
[47] Lü H, Özdemir Ş K, Kuang L M, Nori F and Jing H 2017 *Phys. Rev. Appl.* **8** 044020
[48] Zhang J, Peng B, Özdemir Ş K, Pichler K, Krimer D O, Zhao G M, Nori F, Liu Y X, Rotter S and Yang L 2018 *Nat. Photonics* **12** 479–84
[49] Lü H, Wang C Q, Yang L and Jing H 2018 *Phys. Rev. Appl.* **10** 014006
[50] Wiersig J 2011 *Phys. Rev.* A **84** 063828
[51] Wiersig J 2014 *Phys. Rev. Lett.* **112** 203901
[52] Wiersig J 2016 *Phys. Rev.* A **93** 033809
[53] Xu H, Mason D, Jiang L and Harris J G E 2016 *Nature* **537** 80
[54] Hodaei H, Hassan A U, Wittek S, Garcia-Gracia H, El-Ganainy R, Christodoulides D N and Khajavikhan M 2017 *Nature* **548** 187–91
[55] Peng B, Özdemir Ş K, Lei F, Monifi F, Gianfreda M, Long G L, Fan S, Nori F, Bender C M and Yang L 2014 *Nat. Phys.* **10** 394